Associating Machine-Learning and Analytical Models for QoT Estimation: Combining the Best of Both Worlds

EMMANUEL SEVE[1,*], JELENA PESIC[2], YVAN POINTURIER[3]

[1]*Nokia Bell Labs France, Nozay, Villarceaux, France*
[2]*Nokia IP Optical Networks, Paris-Saclay, Nozay, France*
[3]*Nokia Bell Labs France, Nozay, Villarceaux, France but currently with Huawei, France.*
**Corresponding author: emmanuel.seve@nokia-bell-labs.com*

Received XX Month XXXX; revised XX Month, XXXX; accepted XX Month XXXX; posted XX Month XXXX (Doc. ID XXXXX); published XX Month XXXX

By associating machine-learning and an analytical model (i.e. gaussian noise model), we reduce uncertainties on the output power profile and the noise figure of each amplifier in an optical network. We leverage the Signal-to-Noise Ratio (SNR) of all the light path of an optical network, monitored in all the coherent receivers. The learning process is based on a gradient-descent algorithm where all the uncertain input parameters of the analytical model are iteratively modified from their estimated values to match with the SNR of light paths in a European optical network. The design margin is then reduced to 0.1dB for new traffic demands. © 2020 Nokia Bell Labs.

http://dx.doi.org/10.1364/JOCN.99.09999

1. INTRODUCTION

The design of optical networks relies on a software tool to predict the Quality of Transmission (QoT) such as Bit-Error Rate (BER) for each traffic demand, which must be beyond a predefined threshold. Network designers typically add significant (up to several dBs) pre-defined "design margins" to the values predicted by the QoT tool [1-2], resulting in network over-dimensioning. Design margins compensate for errors both from the QoT physical model itself and from the uncertainties on the tool input parameters.

To improve the accuracy of a QoT tool, many different Machine Learning (ML) algorithms have been considered [3-19]: neural networks, random forest, network kriging, L2-norm minimization, regression, support vector machine. Different sets of network parameters have been considered as inputs for these ML techniques. A detailed review of all these ML methods for the QoT estimation can be found in [20]. In [19], the wavelength allocation of the closest neighbors around the central channel has been included to evaluate the QoT before the traffic demand is established. Experimental validations have been realized in with small-scale network testbeds [21-24].

An accurate ML-aided QoT tool requires a large amount of data for training. Learning the model from a given network topology and applying it to another topology can reduce the need for large training data sets. A transfer learning method can be the solution as shown in [25]. However, for a small amount of uncertainties on the network parameters, it is wiser to keep the analytical models like the Gaussian Model [26] as QoT tool. Indeed, it is shown in [27] that this model is more accurate for the evaluation of the Signal-to-Noise Ratio (SNR) in the area of low uncertainties (on span lengths). The equivalent ML-aided QoT function starts to be more accurate than the analytical model for a larger amount of uncertainties, reducing network design margins. Also, by studying the influence of fiber length uncertainty and its type of distribution (e.g., uniform or gaussian) on the accuracy of the ML-aided QoT estimation, it is shown that a different type of distribution between the actual fiber lengths and the ones considered in the training is also crucial for QoT evaluation [28].

In [29], we proposed a different method to reduce design margins stemming from QoT parameters uncertainties. The goal was to reduce uncertainties on two QoT parameters: Noise Figure (NF) and output power profile of all Erbium Doped Fiber Amplifiers (EDFA) in an optical network. The term "EDFA ouput power profile" is simplified by "power profile" in the rest of this article. Like all these aforementioned ML-aided techniques, our method operated on the same data set to leverage the Signal-to-Noise Ratio (SNR) measurements. The essential difference comes from the fact that we add the information coming from existing analytical models. We do not create a new relation between the SNR and all the network parameters. Indeed, this relation has been already developed and widely tested with experimental data or through (split-step Fourier) simulations. For that reason, we call our approach a "**physicist ML**". The analytical model we considered in this study is the Gaussian Noise model (GN) [30]. In this model, due to the gaussian noise assumption, the inverse of the SNR for all links of the network are all independent (i.e. , no dependency on the path-history of the signal) and can be added to evaluate the SNR of the light path. This property is mandatory for any model correlating the SNR of all established light paths to evaluate the SNR of new light paths. It is also the case for approaches not necessarily based on an analytical model (e.g., [19]), since the additive property of the inverse SNR is also needed.

A similar way to reduce the uncertainties of the QoT tool is proposed in [12]. The authors also iteratively modify the uncertain QoT

parameters. Instead of exploiting the gradient of each parameter to get the new values of the QoT parameters, they modify all parameters by minimizing the difference of the actual and estimated SNR values. This method can be applied to any QoT function (even non-analytical methods), since it does not require the calculation of derivatives. In our method, the gradient is evaluated by deriving the analytical GN formula. However, the gradient can also be obtained with a numerical evaluation of the derivative. It can also work with any QoT tool, such as an empirical QoT function generated with a classical ML method. Our method, like the one presented in [12] is also model-agnostic.

In [27], another approach was introduced to improve the accuracy of SNR estimation in the presence of uncertainties on the span lengths. Like our algorithm, this method combines a ML technique together with an analytical model. First, the SNR is calculated analytically with the uncertain span lengths using the GN model. By feeding a shallow neural network with these SNR values, the error between the nominal values (i.e. measured) and the GN evaluation can be learned and applied to calculate the SNR for new light paths (LPs). By doing so, the SNR is not learned but only the correction to be added to the GN model. This correction is then added to the GN model's SNR estimation.

Any parameter appearing in the SNR analytical formula of the GN model may be uncertain. With a classical ML approach, these uncertainties on QoT parameters also exist, and we would search the unknown relation between the SNR (i.e., output features) and the uncertain QoT parameters (i.e., input features). This relation can be expressed as SNR = f(θ, x) for a ML method based on a single hidden layer neural network; x corresponds to the input features and θ values are the regression parameters. The goal is to find the neural weights θ for a given activation function f, knowing the ML input and output features. The uncertainties on the input parameters (i.e., x) lead to an increase of the inaccuracy of the ML-aided QoT evaluation. For example, the influence of fiber length uncertainty on the accuracy of the QoT estimation was recently analyzed in a classical ML based model [27, 28].

With our **physicist ML** method, the activation function f and the values of coefficients θ are already known since they are given by the analytical model. In that case, we can reduce the uncertainties on the input features "x", knowing the SNR and the model (i.e., θ and f). This procedure cannot be done with a classical ML approach since the activation function is not known. However, a sufficiently accurate analytical model is needed for our **physicist ML** approach. When we have more uncertain input parameters in the model, we can keep our method by extending the list of features. Consequently, we need to re-train our model each time new input features are added. This re-training is also needed for the classical approach when we want to refine the ML model with new features.

The extreme situation where all the terms in the analytical QoT formula are unknown would correspond to the classical ML approach since information on the activation function coming from the analytical model vanishes. A sign of this ML/Analytical model convergence when the uncertainty increases can be seen in [27]: the SNR error of these two approaches tends to the same value for a very large amount of parameter uncertainty (i.e., fiber length uncertainty).

Moreover, the two approaches (physicist or classical) are based on the same inputs and the monitoring of the network parameters can also feed the classical ML algorithm, giving a QoT evaluation more accurate than the one obtained with estimated values of these network parameters (i.e. design values). In the same way, our **physicist ML** approach can also lead to an accurate evaluation of the QoT by starting from the design values of the network parameters, but convergence would be slower. The monitoring complexity is then identical for the classical and **physicist** approach of ML.

In the work initiated in [29], we were assuming that the EDFA output power is flat over the C-band. However, some fluctuations/ripples within the gain bandwidth of the EDFA exist. This non-flatness of the EDFA gain profile has been recently addressed for the (linear) SNR (i.e., OSNR) in [30] and the total SNR (linear + nonlinear) in [31]. In [31] the gain ripple noise penalty for each network connection is estimated at the link level with a supervised ML. This process is fed by the monitoring of the SNR at the receiver side and the estimated gain profiles (at nodes and at each gain equalizer). In [32], we presented an extension of the work presented in [29] to improve the QoT accuracy when the power profile is not flat. The method consists in reducing the uncertainties on the QoT parameters through the addition of additional parameters to characterize the power profile. As in [29], the method is based on a gradient-descent algorithm using correlated information coming from all the established LPs in the optical network. To initiate the process, we use the output of the Automatic Gain Equalizer (AGE), placed just before the transmission fiber to monitor the power profile. This initially inaccurate power profile is then iteratively modified (together with the uncertain NF values) until the QoT evaluation matches with the actual values. With our method, we have access to the power profile at the span level. Compared to [31], the accuracy of the QoT estimation is improved. With 400 LPs, we decrease the error on the QoT for new traffic demands (from few dBs to ~0.1 dB) for the European backbone network thanks to a more accurate QoT tool. This accuracy improvement is coming from the uncertainty reduction of the QoT parameters (NF and power profiles).

In this paper, we extend the work presented in [32] as follows. First, we present new results obtained using first-fit wavelength allocation whereas the random-fit rule was the only rule addressed in [32]. This is an important issue since a part of the allocated C band is different for these two wavelength allocations and it can influence the accuracy of the QoT estimation. Second, we increase the parameter uncertainty variation domain and we observe that the initial knowledge of the QoT parameters has an impact by decreasing slightly and linearly the accuracy with the amount of uncertainty. In our previous work [32], this trend could not be noticed with the two values of uncertainty we considered. Finally, we extend the results with the accuracy of the estimated QoT parameters obtained after the training process by comparing them with the actual values for all the links in the network. A dependency between the QoT parameters accuracy and the number of channels per link is found and helped us understand why the power profile is more accurate for some links.

This paper is organized as follows. We start by describing the algorithm used in our ML procedure to improve the accuracy of the QoT evaluation. After presenting the simulation setup (Section 2) and assumptions (Section 3), our results are presented and separated in three parts.

The first one is devoted to the accuracy improvement of the uncertain QoT parameters at the end of our ML procedure. This step is realized during the greenfield deployment, i.e., at the beginning of the network life. Data is initially collected at that stage to feed our ML algorithm. The second part of the results concerns the validation of the ML process. We validate our improved QoT model with all the demands arriving during the network life (i.e. brownfield deployment). For all these new demands, we show that the accuracy of the SNR evaluation can be as low as 0.1dB. Two types of wavelength allocation are tested: first-fit (Section 4A) and random-fit (Section 4B). In Section 4C, we study the impact of the parameter uncertainty on this improvement of the SNR evaluation.

2. LEARNING PROCESS

The learning process is similar to that of [28]. The difference comes from the presence of additional input parameters in the QoT tool due to the non-flatness of the power profile. The main idea is to modify iteratively the two uncertain QoT parameters (power profile and NF),

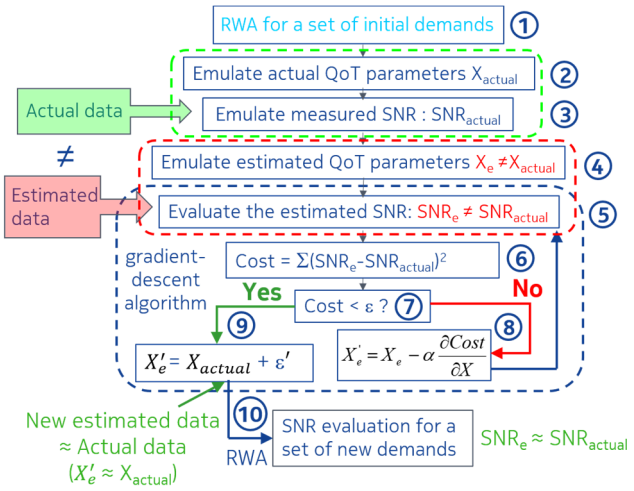

Fig. 1 Block diagram of the learning algorithm. X can be any input parameter of the QoT model.

starting from their estimated values (issued from measurements or from datasheet specifications) until they converge towards the (unknown) actual values. We choose the SNR to characterize the QoT for all traffic demands in the network. The block diagram of our ML is illustrated in Fig. 1 and the different steps of the algorithm are the following:

①We start by a routing and wavelength assignment (RWA) for a set of initial demands. The RWA process is realized with a Random Fit (RF) or a First Fit (FF) wavelength allocation as described further.

②Numerical emulation for the actual values of the QoT parameters (all measured power profiles and the noise figure for all EDFAs): X_{actual} (in Fig. 1). The goal of our ML algorithm is to recover these unknown values with the smallest amount of traffic.

③From X_{actual}, we evaluate the actual SNR of all initial demands (greenfield deployment, i.e., first established services) using the analytical QoT model (i.e., GN model): SNR_{actual}.

④Numerical emulation for the estimated values of the QoT parameters: X_e. These values constitute the starting point of our iterative ML process.

⑤From these estimated values X_e, we evaluate the estimated SNR (SNR_e) using the same analytical QoT model.

Due to the uncertainties on the estimated parameters X_e, the estimated SNR is different from the actual one: $SNR_e \neq SNR_{actual}$. We assume that the uncertainty on the measured SNR is much lower than that arising from the power profile and the noise figure of all the EDFAs. Therefore, the actual SNR (SNR_{actual}) corresponds to the ground-truth values in our simulations. The accuracy of the analytical model will be discussed in Section 3.

⑥Construction of the cost function defined with the following expression: $Cost = \Sigma(SNR_e - SNR_{actual})^2$.

The summation in the expression of the cost function is realized over all the LPs in the training set to correlate all the available information in the network.

⑦We test if the cost function Cost is below a predefined threshold ε.

⑧When Cost >= ε, initial values of the QoT estimated parameters (X_e) are then modified iteratively by a fixed fraction (α) of the cost function gradient with respect to each QoT parameter (X'_e).

⑨When Cost < ε, the new estimated QoT parameters X'_e are then close to the actual values: $X'_e = X_{actual}$ and we interrupt the ML process.

⑩Using the new converged power profiles and NF values, we can evaluate more accurately the QoT of new traffic demands: $SNR_e \approx SNR_{actual}$.

If we update the training database with information coming from new demands, the QoT prediction tool may be refined through re-training. Since there is no dependency between the parameters of all power profiles, the gradient of each QoT parameter is independently evaluated for each span. We average over all light paths passing through each span at each step of the iterative process of the gradient-descent algorithm.

The QoT model we consider (GN) is completely analytical: it has the advantage to be approximated by a closed form giving the nonlinear variance for one light path and for any wavelength allocation, as given by the following expression:

$$\sigma_{NL} = \sum_{k=1}^{N} \sigma_k \ , \sigma_k = \sigma_k^{SPM} + \sigma_k^{XPM} \tag{1}$$

The summation is done over all N spans in the light path due to the additive property of the gaussian noise. The nonlinear SNR of the span k (σ_k) is the sum of two terms: the self- and the cross-phase modulation contribution, named SPM and XPM, respectively. With the GN model, SPM and XPM contributions of the nonlinear distortion σ_k take the following analytical form for the channel j and the span k [26]:

$$\sigma_k^{SPM} = A_k \ \mathrm{asinh}\left(C_k \ B_j^2\right) P_{j,k}^2 \tag{2}$$

$$\sigma_k^{XPM} = \sum_{i=1}^{N_{ch}} A_k \left[\mathrm{asinh}\left(C_k \left[f_i - f_j + \frac{B_i}{2}\right] B_j\right) - \mathrm{asinh}\left(C_k \left[f_i - f_j - \frac{B_i}{2}\right] B_j\right)\right] P_{i,k} P_{j,k}. \tag{3}$$

$$A_k = f(L, \alpha, D, \gamma), \quad C_k = g(L, \alpha, D) \tag{4}$$

In Eq.(3), the summation corresponds to the contribution of all channels i (frequency f_i , power $P_{i,k}$) aside studied channel j (frequency f_j , power $P_{j,k}$) in the span k. N_{ch} is the total number of channels. $B_{i,j}$ is the baud rate of channel i and j. Terms A_k and C_k depend on the physical characteristics of the span k: length L, attenuation α, local dispersion D and nonlinear coefficient γ. The expression of the functions f and g can be found in Eq. (128) of [26].

The total SNR (i.e. the measured one) is given by the formula:

$$\frac{1}{SNR} = \frac{1}{OSNR} + \frac{1}{SNR_{NL}} \tag{5}$$

where the linear part of the SNR (i.e. OSNR) is given by:

$$\frac{1}{OSNR} = h\nu \cdot B_{ref} \cdot e^{\alpha L} \sum_{k=2}^{N} \frac{NF_k}{P_{j,k}} = \sum_{k=1}^{N} A_k \frac{NF_k}{P_{j,k}} \tag{6}$$

B_{ref} is the reference spectral bandwidth, h is the Planck constant and ν the optical frequency.

The nonlinear SNR (SNR_{NL}) is given by the inverse of the nonlinear noise variance σ_{NL}.

As mentioned in the introduction, we can have some uncertainties on all terms appearing in the SNR expression (1)-(6), but we are focusing on the uncertainty on the channel

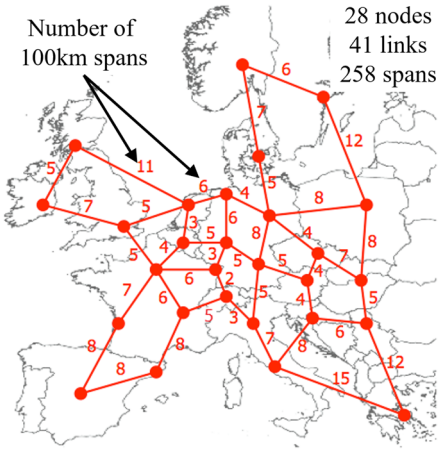

Fig. 2 European network topology [33]

power of each channel ($P_{i,k}$ or $P_{j,k}$) and on the EDFA noise figures NF_k.

3. SIMULATION SETUP AND ASSUMPTIONS

In all our simulations, we consider the case of a European network consisting of M = 28 nodes, 41 dispersion uncompensated links and 258 spans, as illustrated in Fig. 2. Since all these spans are unidirectional, there are 516 standard SMF unidirectional fibers in the network [33]. The established demands are carried with 28Gbaud PDM-QPSK modulated wavelengths, yielding 100Gb/s net bitrate. For these demands, there are M(M-1) = 756 possible connections between the M = 28 nodes. A fixed grid of 50GHz was considered in these simulations. This work could be easily adapted for a flex grid wavelength allocation. For the greenfield deployment phase, we consider a uniform traffic matrix where all connections are chosen with equal probability among the M(M-1) = 756 possible source/destination connections. We use Dijkstra's algorithm to find the shortest path and two types of wavelength allocation: random and first-fit rules. For the first-fit rule, the allocated wavelength for each demand is the first one in the spectrum which is commonly available for all the links of the light path. If no wavelength is available, the demand is dropped. The wavelength choice in the random-fit rule is equivalent to the first-fit rule except that the wavelength is chosen randomly in all the available spectrum. Since the reach of our 100Gb/s demands is higher than the longest LP, we can assume that all demands are carried transparently. We also assume that wavelength-dependence of the received SNR has no impact in the system reach. Associating the wavelength with the highest SNR to the longest LP is not considered in this study.

To illustrate the assumption that the EDFA output profiles are not flat in terms of wavelength, in Fig. 3 we show an example of power profile as function of the 80 wavelength slots of 50GHz in the C-band. In this study, we consider that the shape of the power profile is sinusoidal. The solid curve corresponds to the actual shape. The dot-dashed is the measured power profile, the one which is the starting point of our gradient-descent algorithm. Finally, the dashed one corresponds to the estimated power profile obtained at the end the ML process. The objective of our **physicist ML** process is to converge the measured power profile towards the actual power profile, giving the estimated power profile at the end of the learning process. Each curve is characterized by three independent parameters: the average power (A), the amplitude (B) and the wavelength peak shift (C) measured from the first wavelength of the C-band (cf. Fig. 3).

Table 1 Emulation of the actual and estimated values. *One AGE per span: the amplitude B is 1 dB for all the spans of the link. **One AGE per link: the amplitude B increases by 1 dB after each span of the link until the AGE is reached

QoT param.	Actual values	Estimated values
A	$\{A_a\}$=U[0.75, 1.25]	$\{A_e\}=\{A_a\}$+U[-Δ, Δ]
B	$\{B_a\}$=1dB * or $\{B_a\}$+ =1dB **	$\{B_e\}=\{B_a\}$+U[0 , Δ]
C	$\{C_a\}$=21	$\{C_e\}=\{C_a\}$ +U[0 , Δ]
NF	$\{NF_a\}$=U[5.5, 6.5]dB	$\{NF_e\}$ = 5dB

For an arbitrary power profile different for each EDFA output, we tested the gradient-descent algorithm on the coefficients of a polynomial expansion of the power profile. There are two drawbacks to this approach. Firstly, the polynomial degree is very large to reproduce any shape of power profile. Secondly, the polynomial shape is also extremely sensitive with a small change in the polynomial coefficients. Consequently, it is difficult to be used with a gradient-descent algorithm. In that case, other techniques can be investigated but the general idea of modifying the power profiles with successive iterations to match with the SNR measurements developed in this article can remain the same.

The way we generate the actual and estimated values is shown in Table 1. For actual values, we consider a uniform distribution, U[min, max], for the averaged power A and NF: U[0.75, 1.25] dB and U[5.5, 6.5] dB; and constant values for B and C: 1 dB and 21 wavelength slots. To equalize the power profile, an AGE was placed either after each span of the network or only after the last EDFA on the link. The power equalization is considered as perfect (no amplitude ripple after the AGE). These two configurations will be named in the text with the expression "one AGE per span" or "one AGE per link". As shown in Table 1, the actual value of the amplitude B is constant when we consider one AGE per span: $\{B_a\}$ = 1dB and increases by 1dB after each EDFA until the AGE is reached ($\{B_a\}$ + = 1dB) when we consider one AGE per link. The choice of this linear +1dB amplitude increasing at each EDFA could be replaced with any non-linearly increasing function. However, we would keep this order of magnitude for the amplitude growth according to what is commonly observed in real networks. For

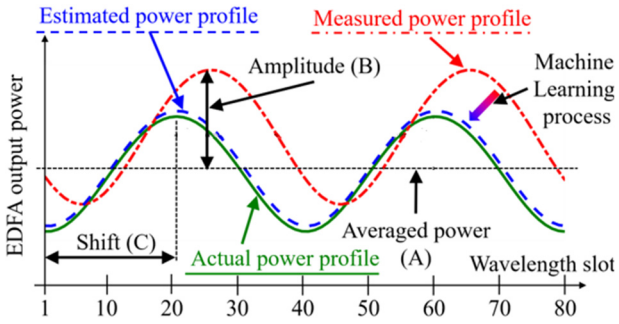

Fig. 3 Illustration of the power profile convergence: from the measured profile (dot-dashed curve) to the estimated one (dashed curve).

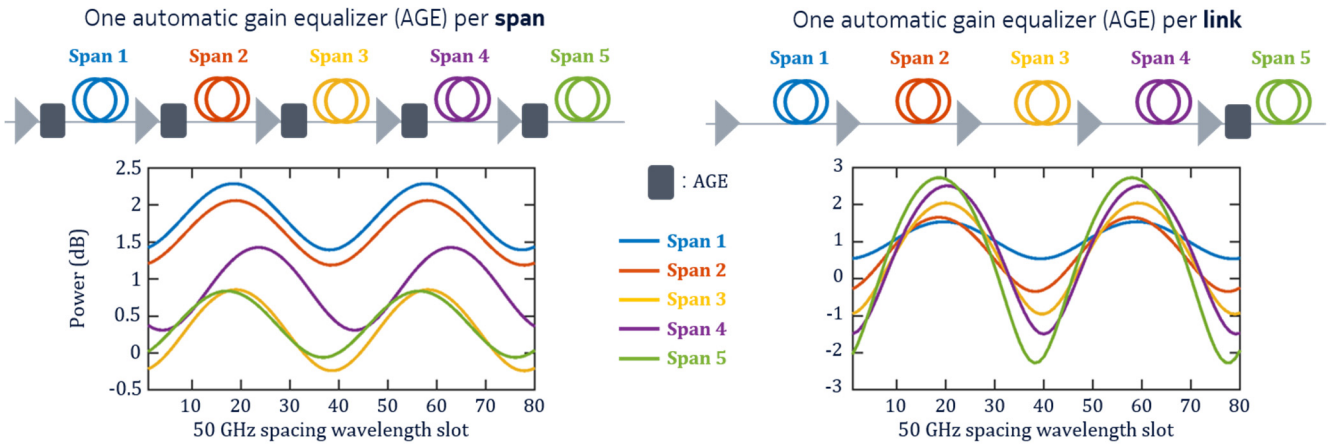

Fig. 4 Example of power profile for a 5-spans link. Left: one AGE per span. Right: one AGE per link.

the case "one AGE per link", the AGE is positioned after the last EDFA on the link. As we can see in the last column of Table 1, the parameters of all the measured power profiles are emulated by adding a zero-mean uniform noise around each actual value (U[-Δ, Δ]), emulating monitoring inaccuracy. We show in Fig. 4 an example of the estimated power profiles at the entrance of the equalizer for all spans of a link in these two AGE configurations. Fig. 4 (left): one AGE per span and Fig. 4 (right): one AGE per link. With one AGE per span, all these profiles can be measured (at the output of the AGE) and the amplitude is equal to 1 dB for all 5 spans. In this example, only the value of the average power A and the wavelength peak shift C varies from one span to another. The amplitude B is kept constant in this example in order to make a clear comparison with the case of one AGE per link. With one AGE per link, only the last power profile (the 5th in our example) can be obtained. In the absence of AGE for the other spans, we do not have any information on the estimated power profile. To initiate the gradient-descent algorithm, we start from the only measured profile (i.e. the output of the AGE for the last span on the link) and we scale the shape with a homothetic transformation: we only decrease regularly the amplitude B. For example, if 5 dB is the measured amplitude for the 5th and last span, we keep the same global shape, but we assume that the missing amplitude for the other spans varies by 1dB after each span. Several values of uncertainties are tested. The initial NF values are taken from datasheets specifications. Three values of NF (5, 6 and 7 dB) are considered to start the ML process.

To compose our training set for the greenfield deployment, we consider several numbers of LP (N^{LP}, from 100 to 1000) and each of them is randomly and uniformly chosen among the 756x80 possible route/wavelength slots combinations. By constructing a set of LPs this way, a demand with the same source/destination can be repeated but with different wavelength allocation. The cumulated capacity for this source/destination is then a multiple of 100 Gb/s. For each value of N^{LP}, 10 random selections of LPs are considered with a uniform distribution

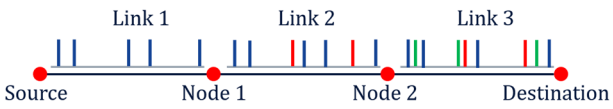

Fig. 5. Example of wavelength allocation for a 3-links light path. The blue bars correspond to the wavelengths present for all links. The red and green bars correspond to the wavelength added in node 1 and 2, respectively.

of the traffic matrix inside the network. An example of the wavelength allocation is displayed in Fig. 5 for a 3-links light path. The added wavelengths coming from other routes and sharing some common links, inserted at node 1 and 2, are represented by red and green vertical bars, respectively. In this example, we illustrate also that the wavelength allocation may differ from one link to another one. It is valid for a random- or first-fit wavelength allocation rule.

Since the wavelength allocation changes each time a new wavelength is added in the network during the testing part of the ML process, it is important to include the information on the exact wavelengths position in the QoT model. In Fig. 6, we show the probability of over-estimation of the SNR when considering a full wavelength occupancy with respect to the real one for a random set of 1000 light paths established in our network. The SNR can be over-estimated by as much as 5 dB and the average value is 1.7 dB (see the red dashed line). In the inset, we plot the complement of the cumulated probability as function of the SNR difference. The SNR over-estimation of 76% of the 1000 light paths is larger than 1dB. Learning the QoT rule from existing LPs and applying it for all testing (new) light paths, for which the wavelength allocation is different, can lead to an over estimation of the throughput or to a minimization of the number of regenerators. Indeed, if we elaborate the QoT model with the assumption that the spectrum is fully occupied for all light paths in the training and testing set, it leads to a SNR lower than the actual values since the spectrum occupancy increases for all the new established light paths and this change of occupancy has not been learned. In addition, this under-estimation of the SNR also applies on the previously established light paths since the number of neighboring wavelengths has increased in the meantime. To overcome this situation, the wavelength allocation should be added among the features of any ML algorithm. This feature has been included in [19] to account for the correlation in both space and spectrum domains to evaluate the QoT of demands before being established. The set of data can be extremely large since it should contain all the possible wavelength allocations. To reduce the amount of data, which is exponential with the number of wavelengths, the authors have considered a maximum of three neighboring channels aside the central one. More, each time we need to add wavelength-dependent QoT parameters, like the power or the baud-rate (e.g., for an elastic network), the amount of data strongly increases. In our method, this wavelength allocation is already present since we consider the GN analytical model as a part of the information we use for the ML process. Consequently, we don't need to learn these neighboring channels interference. However, unlike what is presented in [19], the QoT accuracy in our approach strongly depends on the

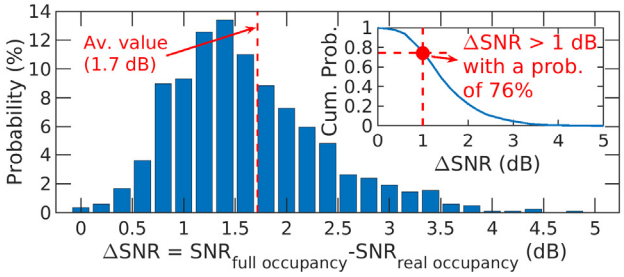

Fig. 6. Probability of the SNR error with a full wavelength occupancy with respect to the real wavelength occupancy with one random set of 1000 light paths.

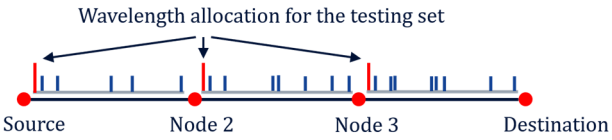

Fig. 7. Example of wavelength allocation for a 3-links light path. The blue bars correspond to the wavelengths in the greenfield deployment (training phase). The red bars correspond to the new wavelengths added in the brownfield deployment (testing phase).

accuracy of the analytical model. On the other hand, the inaccuracy due to the non-additivity of the inverse SNR at the link level is common for both approaches and for any other method leveraging the QoT. The error due to a non-gaussian distribution of the nonlinear noise variance (σ_{NL}) has been evaluated to less than 2dB, depending on the number of channels or fiber type in [34]. Knowing that the installed systems are operating few dBs below the optimal power to avoid uncorrected blocks and using the Eqs. (1)-(6), the SNR error is around 0.27dB for a shift of -2dB. This QoT inaccuracy is much lower than the several dBs design margin which is usually considered [1-2].

After this training process, we obtain the power profiles and NF values for all spans close to the actual ones. We need to validate them by considering new light paths for which we calculate a route, assign wavelengths and calculate the QoT using the new converged power profiles and NF values. This phase corresponds to the brownfield deployment in the network life. An example of wavelength assignment for one light path is illustrated on Fig. 7. The blue vertical bars represent all assigned wavelengths for the light paths initially established and belonging to the training set (greenfield deployment). The red vertical bar represents the wavelength allocation for the new light path (brownfield deployment).

Adding new light paths in the brownfield deployment can modify the EDFA output profile obtained during the phase of training in a dynamic scenario, even in the case where the new wavelengths are allocated between the previously established one. To tackle this issue, a step composed with an EDFA gain modeling can be added after the training phase to consider this power profile changes between the training and testing phases. A lot of studies have been published on that subject, for EDFAs or Raman amplifiers [35-48]. A re-training can be realized at any time during the brownfield deployment to adjust this estimated power profile with the same ML procedure previously presented. Obviously, it is difficult to extrapolate the power for wavelengths far away from the highest wavelength of previously established demands in the greenfield deployment. The best way is to treat these demands separately. For example, we can set their powers to the average value of the power profile obtained with our ML approach and refine these values with a re-training.

To widely test the ML-aided QoT rule, we consider all possible combinations of source/destination of our network and for each of them, we calculate the shortest-path route. For all available wavelengths of each light path (i.e., each empty slot in Fig. 7), we evaluate the SNR ($SNR_{estimated}$) and compare it to SNR_{actual} calculated with the actual values of the QoT parameters. The accuracy of our ML method is then defined as a difference between $SNR_{estimated}$ and SNR_{actual}.

4. RESULTS

A. Reduced uncertainties on the QoT parameters

In Fig. 8, we show the evolution of the error on all estimated QoT parameters {A, B, C, NF} as function of the number of iterations during the gradient-descent process for one random set of 1000 training LPs using the random-fit wavelength allocation. We consider a typical 5-spans link from the network. There were 10^6 iterations in the ML process, taking about one hour on a standard desktop PC without any optimization, scaling linearly with the number of LPs. Before all QoT parameters converge towards the actual values at the end of the ML process, the error reduction follows a path which is completely different for the QoT parameters of each span. It shows that all parameters of the gradient-descent algorithm are free to evolve, as mentioned earlier in the method description. In Fig. 8(a) we even see that the error on the parameter A starts to decrease for some spans in the link (i.e. 1 and 2) and increase for the other spans (3, 4 and 5). At the end of the process, they all converge to the actual values.

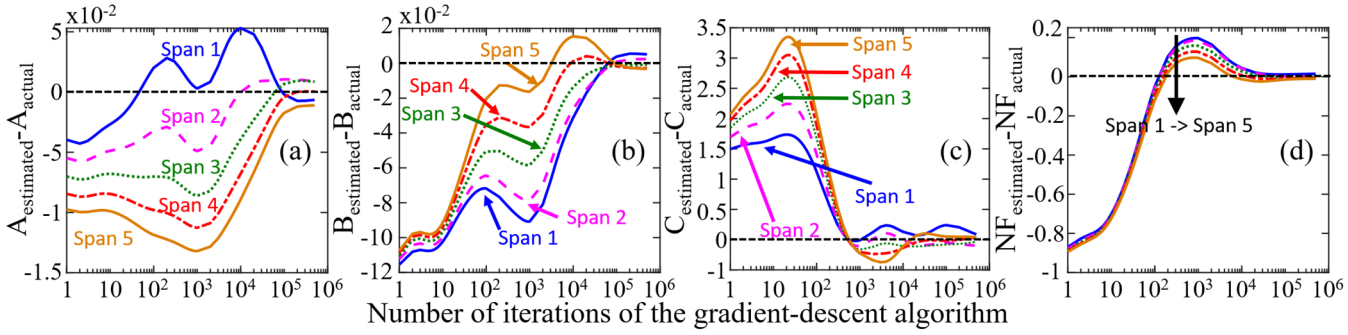

Fig. 8 (a), (b) and (c): Evolution of the error (estimated-actual, linear scale) during the gradient-descent algorithm on the EDFA output power profile of one typical link (made of 5 spans): on the averaged power A, the amplitude B and the wavelength shift C. (d): on the NF.

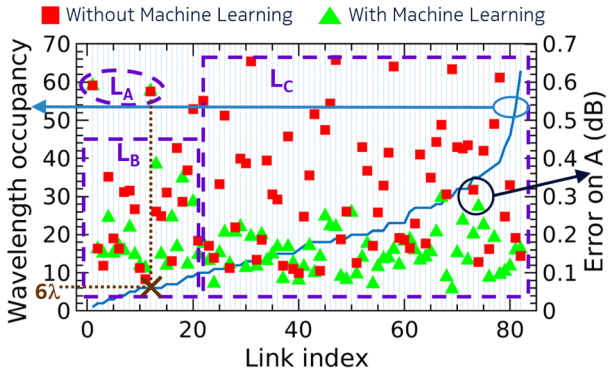

Fig. 9 Error on the parameter A (see Fig. 3) for all the 82 network unidirectional links sorted with an increasing wavelength occupancy (i.e. the number of wavelengths in the spectrum) and for a random-fit wavelength allocation. This wavelength occupancy is represented by the blue curve and its scale is shown on the left y-axis. The error on the parameter A (in dB) is represented with green triangles (with ML) and the with red squares (without ML).

This error reduction on the QoT parameters may vary for each network link. For that purpose, we plot in Fig. 9 the error on the parameter A (see Fig. 3) for all network links sorted with an increasing wavelength occupancy (i.e. the number of occupied wavelengths in the spectrum) and for a random-fit wavelength allocation. As all spans are unidirectional, the wavelength allocation is then different for both directions; explaining why the number of links on the x-axis goes up to 82. This wavelength occupancy is represented by the blue curve and its scale is shown on the left y-axis. The error on the parameter A (in dB) is represented with green triangles (with ML) and the with red squares (without ML). We have divided the figure in three parts: L_A, L_B and L_C. In the part "L_A" (consisting of link 1 and 12), the largest error is around 0.6 dB, with and without ML. For these two links, the wavelength occupancy is extremely low: only 6 wavelengths in the complete C-band (brown cross in Fig. 9). In the part "L_B" (links 2 to 20, except 12), the error is lower than in "L_A", but we still have a similar error, with and without ML. A prediction of the complete power profile based on only few points necessarily introduces discrepancies. On the contrary, in the part "L_C", the number of allocated wavelengths is larger than 20, leading to a better fit of the power profile and the error obtained with ML is globally much lower than the one obtained without ML. The error on the parameter A of the power profile (i.e. amplitude) is always lower than 0.3 dB once the ML process is achieved. Without this ML process, it can reach 0.7 dB.

B. *Reduced QoT inaccuracy (random-fit wavelength allocation)*

With accurate power profiles and NF values at the end of the ML process, we evaluate the SNR for all new traffic demands. This testing set for our ML algorithm is built as follows: for each traffic matrix at the end of the greenfield deployment, we list all possible LPs for which we have a possible wavelength to be allocated. The testing set is the complementary part of the training set. The ratio between the amount of training data with respect to the total value (training + testing) is equal to [0.2; 0.5; 1.6; 10.6] %, well below the usual 70% used in ML method. This learning ratio is shown on the top horizontal scale for each sub-figure of Fig. 10. For each LP from this testing set, we evaluate the SNR using the GN model fed by the QoT parameters obtained either with the ML process ($SNR_{estimated}$) or by using the actual values (SNR_{actual}).

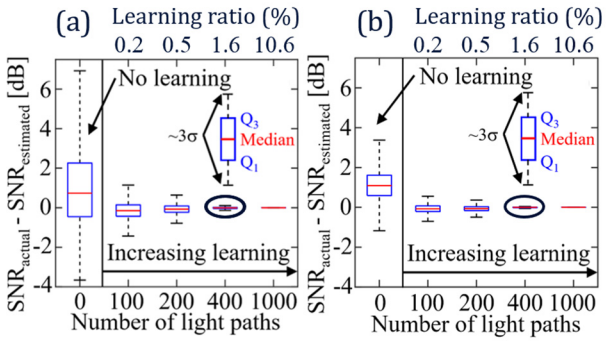

Fig. 10 Box plots of the SNR error without and with ML as function of the number of light paths in the training set for a parameter uncertainty Δ of 1 dB. (a): one AGE per link. (b): one AGE per span. The top horizontal scale is the corresponding learning ratio (random-fit allocation).

Fig. 10 represents the box plot of the SNR error (SNR_{actual} - $SNR_{estimated}$) as function of the number of training LPs (from 100 to 1000). Each box plot is defined by 3σ, median, first (Q1) and third (Q3) quartile values. The case of one AGE per link/span is shown in Fig. 10(a)/ Fig. 10(b), respectively. We consider Δ = 1dB of uncertainty on all the QoT parameters.

With such uncertainty on the power profile parameters, the SNR error is in the range [-4, 6] dB with one AGE per link and [-1, 3] dB with one AGE per span. As mentioned before in Section 3, with one AGE per link, only the power profile of the last span of the link is known and all others are inferred, leading to a strong uncertainty on the power profiles for all spans except for the last one. Consequently, the SNR error can be extremely large without our ML process, as we can see in Fig. 10(a). However, with one AGE per link or per span, the SNR error decreases rapidly when we increase the size of the training set: the SNR error is reduced to ~0.1 dB for 99.7% of cases (3σ) with only 400 light paths (1.6% of learning/testing ratio). Hence, the excess of uncertainties in the power profile with one AGE per link almost vanishes with the ML process.

C. *Reduced QoT inaccuracy (first-fit wavelength allocation)*

Focusing now on the impact of the wavelength allocation, we compare in Fig. 11 the SNR error obtained after the ML process for two wavelength allocation rules: RF and FF. Like in Fig. 10, we

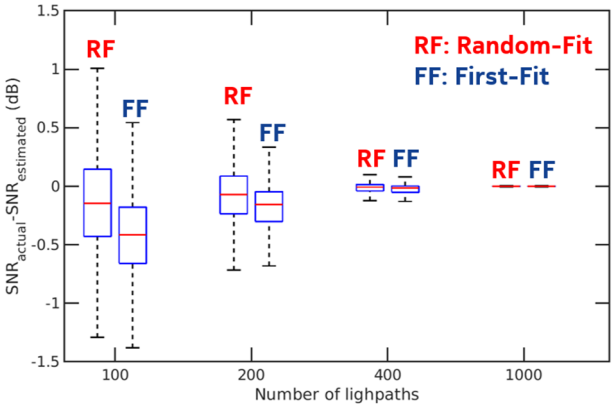

Fig. 11. Box plot the SNR error as function of the number of training LPs (from 100 to 1000) for the two types of wavelength allocation: RF and FF, respectively.

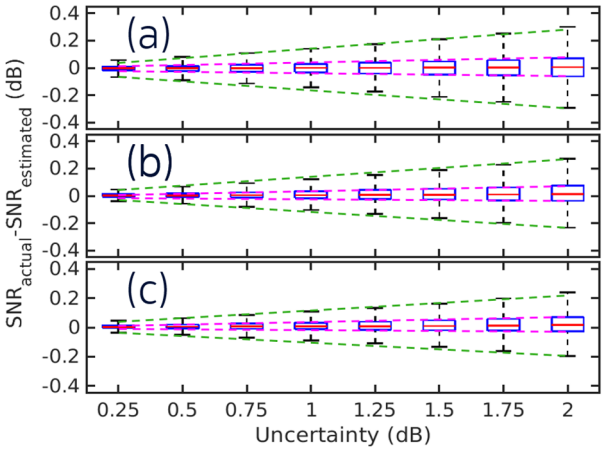

Fig. 12. SNR error box plot as function of the uncertainty on the power profile parameters and for three estimated values of NF: 5 dB (a), 6 dB (b) and 7 dB (c). These results are obtained for 400 light paths and with one AGE per link

plot the box plot the SNR error (SNR_{actual} - $SNR_{estimated}$) as function of the number of training LPs (from 100 to 1000). We focus on the worst situation: one AGE per link and with 1dB of uncertainties on the parameters of the power profile. For both wavelength allocations, the SNR error is reduced in a similar way when we increase the number of light paths in the training set: 400 light paths are required to reduce the QoT inaccuracy to less than 0.15 dB. The accuracy obtained during the ML process is even slightly lower with the first-fit allocation, due to a denser repartition of data in the first half of the power profile. With a more complex and non-symmetric power profile, we would obtain a similar accuracy level with a high number of light paths or with a random-fit wavelengths allocation.

D. Impact of the amount of uncertainties

To recover the actual shape of the power profile at the EDFA output, we start by estimating this shape with measurements available at the output of the AGE. To study the impact of the discrepancy between the actual and the estimated values of the input QoT parameters, we show in Fig. 12 the SNR error box plot as a function of the uncertainty on the power profile parameters and for three estimated NF values: 5 dB (a), 6 dB (b) and 7 dB (c). These results are obtained with 400 light paths and with one AGE per link. The QoT estimation after the ML process is always very accurate since the SNR error reaches only 0.3 dB when the uncertainty on each QoT parameter can be as high as 2dB. For each estimation of the NF values (5, 6 or 7 dB), the SNR error evolves linearly with the amount of uncertainty, for the 3σ and the average value, as shown by the green and red dashed lines in all the subplots of Fig. 12. The small decrease of the SNR error with the actual value of the NF can be attributed to a reduction of the nonlinear noise variance (which is P^2 dependent) with respect to the linear variance (which is P^{-1} dependent); P is the average power of the power profile. Indeed, the average ratio of the nonlinear variance over the total value (Eq. 5) is decreasing from 0.56 to 0.45 when the NF varies from 5 to 7dB.

5. CONCLUSION

To obtain an accurate QoT model, there are two options. The first solution is to use ML techniques to build the function relating the monitored SNR to the network characteristics. The second solution (considered in this article) is to improve the accuracy of the SNR evaluated with an analytical QoT model (GN) by reducing the uncertainties on its input parameters. In this work, we are focusing on two input parameters: the output power profile and the noise figure for all the EDFA amplifiers in the network. By feeding a machine-learning process based on a gradient-descent algorithm with a set of measured/monitored data (SNR, EDFA output power profile) and NF values issued from datasheets, we were able to reduce those uncertainties. Consequently, we reduce design margins from a few dBs to about 0.1dB for new demands in the brownfield scenario of a European network topology. The over-provisioning can be strongly reduced, decreasing the cost of the network. To reach such a level of accuracy, we assumed that the GN model gives the ground-truth SNR. The analytical QoT model should be sufficiently accurate at least when there are no uncertainties on the network parameters. In that case, our physicist ML is a promising direction to improve the QoT evaluation by decreasing the parameters uncertainties using the SNR monitoring. More, to reduce this additional QoT evaluation error due to the non-additivity of the inverse SNR, we should keep working on improving the analytical models. Analytical network modeling and ML-based approaches join their forces to improve the existing models.

References

1. Y. Pointurier, “Design of low-margin optical networks”, J. Opt. Commun. Netw., Vol. **9**, no. 1, pp. 9-17 (2017).
2. J-L. Augé, “Can we use flexible transponders to reduce margins?”, in *Optical Fiber Communication Conference* (2013), paper OTu2A1.
3. L. Barletta, A. Giusti, C. Rottondi and M. Tornatore, "QoT estimation for unestablished lighpaths using machine learning", in *Optical Fiber Communication Conference* (2017), paper Th1J.1.
4. I. Sartzetakis, K. Christodoulopoulos and E. Varvarigos, "Formulating QoT Estimation with Machine Learning" in *European Conference on Optical Communication* (2018).
5. C. Rottondi, L. Barletta, A. Giusti and M. Tornatore, "Machine-learning method for quality of transmission prediction of unestablished lightpaths" in IEEE/OSA Journal of Optical Communications and Networking, vol. 10, no. 2, pp. A286-A297, Feb. 2018.
6. T. Tanimura, T. Hoshida, T. Kato, S. Watanabe, and H. Morikawa, "Data-analytics-based Optical Performance Monitoring Technique for Optical Transport Networks," in *Optical Fiber Communication Conference* (2018), paper Tu3E.3.
7. R. M. Morais and J. Pedro, "Machine learning models for estimating quality of transmission in DWDM networks," in IEEE/OSA Journal of Optical Communications and Networking, vol. 10, no. 10, pp. 84-99, Oct. 2018.
8. M. Zhang, D. Fu, B. Xu, B. Wu and K. Qiu, "QoT estimation for Unestablished Lightpaths Using Artificial Neural Networks," in *Conference on Lasers and Electro-Optics* (2018).
9. W. Mo, Y. Huang, S. Zhang, E. Ip, D. C. Kilper, Y. Aono, and T. Tajima, "ANN-Based Transfer Learning for QoT Prediction in Real-Time Mixed Line-Rate Systems," in *Optical Fiber Communication Conference* (2018), paper W4F.3.
10. Tremblay, C.; Allogba, S.; Aladin, S., "Quality of Transmission Estimation and Performance Prediction of Lightpaths Using Machine Learning", *European Conference on Optical Communication* (2019).
11. Gao, Z, Yan, S, Zhang, J, Mascarenhas, M, Nejabati, R, Ji, Y & Simeonidou, D, 2019, ‘ANN-Based Multi-Channel QOT-Prediction over A 563.4-KM Field-Trial Testbed’, in *European Conference on Optical Communication* (2018).
12. I. Sartzetakis, K. K. Christodoulopoulos and E. M. Varvarigos, "Accurate quality of transmission estimation with machine learning," in IEEE/OSA Journal of Optical Communications and Networking, vol. 11, no. 3, pp. 140-150, March 2019.

13. D. Azzimonti, C. Rottondi and M. Tornatore, “Using Active Learning to Decrease Probes for QoT Estimation in Optical Networks” in *Optical Fiber Communication Conference (2019)*.
14. T. Panayiotou, G. Savva, B. Shariati, I. Tomkos and G. Ellinas, "Machine Learning for QoT Estimation of Unseen Optical Network States," in *Optical Fiber Communications Conference* (2019).
15. D. Azzimonti, C. Rottondi, and M. Tornatore, "Reducing probes for quality of transmission estimation in optical networks with active learning," J. Opt. Commun. Netw. 12, A38-A48 (2020).
16. R. M. Morais, B. Pereira, and J. Pedro, "Fast and High-Precision Optical Performance Evaluation for Cognitive Optical Networks," in *Optical Fiber Communication Conference* (2020), paper Th3D.3.
17. A. D. Shiner, M. E. Mousa-Pasandi, M. Qiu, M. A. Reimer, E. Y. Park, M. Hubbard, Q. Zhuge, F. J. Vaquero Caballero, and M. O’Sullivan, "Neural Network Training for OSNR Estimation From Prototype to Product" in *Optical Fiber Communication Conference* (2020), paper M4E.2.
18. N. Sambo, Y. Pointurier, F. Cugini, L. Valcarenghi, P. Castoldi, I. Tomkos, “Lightpath establishment assisted by offline QoT estimation in transparent optical networks”, J. Opt. Commun. Netw. Vol. 2, no 11, pp 928-937 (2010).
19. I. Sartzetakis, K. Christodoulopoulos, C. P. Tsekrekos, D. Syvridis, E. Varvarigos, “Quality of Transmission in WDM and elastic optical networks accounting for space-spectrum dependencies”, J. Opt. Commun. Netw. Vol. 8, no 9, pp 676-688 (2016).
20. F. Musumeci, C. Rottondi, A. Nag, I. Macaluso, D. Zibar, M. Ruffini and M. Tornatore, “An Overview on Application of Machine Learning Techniques in Optical Networks”, IEEE Comm. Surveys & Tutorials, vol. 21, n°2, 2019.
21. S. Oda, M. Miyabe, S. Yoshida, T. Katagiri, Y. Aoki, J. C. Rasmussen, M. Birk, K. Tse, “A learning living network for open ROADM networks”, in *European Conference on Optical Communication* (2016), paper Tu2B1.
22. Q. Fan, J. Lu, G. Zhou, D. Zeng, C. Guo, L. Lu, J. Li, C. Xie, C. Lu, F. N. Khan, and A. P. T. Lau, "Experimental Comparisons between Machine Learning and Analytical Models for QoT Estimations in WDM Systems," in *Optical Fiber Communication Conference* (2020), paper M2J.2.
23. R. Proietti, X. Chen, K. Zhang, G. Liu, M. Shamsabardeh, A. Castro, L. Velasco, Z. Zhu, and S. J. Ben Yoo, "Experimental Demonstration of Machine-Learning-Aided QoT Estimation in Multi-Domain Elastic Optical Networks with Alien Wavelengths," J. Opt. Commun. Netw. 11, A1-A10 (2019).
24. M. Bouda, S. Oda, Y. Akiyama, D. Paunovic, T. Hoshida, P. Palacharla, and T. Ikeuchi, "Demonstration of Continuous Improvement in Open Optical Network Design by QoT Prediction using Machine Learning," in *Optical Fiber Communication Conference* (2019), paper M3Z.2.
25. J. Pesic, M. Lonardi, T. Zami, N. Rossi and E. Seve, “Transfer Learning Using ANN for G-OSNR Estimation in WDM Network Topologies”, in *Advanced Photonics Congress* (2020).
26. P. Poggiolini, G. Bosco, A. Carena, V. Curri, Y. Jiang, F. Forghieri, “A Detailed Analytical Derivation of the GN model of Non-linear Interference in Coherent Optical Transmission Systems”, arXiv.org, 1209.0394, v13, 6 June 2014.
27. M. Lonardi, T. Zami, N. Rossi and J. Pesic. “The Perks of Using Machine Learning for QoT Estimation with Uncertain Network Parameters”, in *Advanced Photonics Congress* (2020).
28. J. Pesic, M. Lonardi, N. Rossi, T. Zami, E. Seve, and Y. Pointurier, “How uncertainty on the fiber span lengths influences QoT estimation using machine learning in WDM networks”, in *Optical Fiber Communication Conference* (2020), paper Th3D5.
29. E. Seve, J. Pesic, C. Delezoide, S. Bigo and Y. Pointurier, “Learning process for reducing uncertainties on network parameters and design margins”, J. Opt. Commun. Netw. Vol. 10, no 2, pp 298-306 (2018).
30. A. D’Amico, S. Straullu, A. Nespola, I. Khan, E. London, E. Virgillito, A. Tanzi, G. Galimberti, and V. Curri, “Using machine learning in an open optical line system controller”, J. Opt. Commun. Netw. Vol. 12, no 6, pp C1-C11 (2020).
31. A. Mahajan, K. Christodoulopoulos, R. Martínez, S. Spadaro and R. Muñoz, “Modeling EDFA Gain Ripple and Filter Penalties with Machine Learning for Accurate QoT Estimation”, J. Lightwave. Technol, Vol. 38, no 9, pp 2616-2629 (2020).
32. E. Seve, J. Pesic and Y. Pointurier, “Accurate QoT Estimation by Means of a Reduction of EDFA Characteristics Uncertainties with Machine Learning”, in *Optical Network Design and Modeling* (2020).
33. http://sndlib.zib.de/home.action
34. P. Poggiolini, G. Bosco, A. Carena, V. Curri, Y. Jiang, F. Forghieri, “A Simple and Effective Closed-Form GN Model Correction Formula Accounting for Signal Non-Gaussian Distribution”, J. Lightwave. Technol., Vol. 33, no. 2, pp. 459-473 (2015).
35. X. Ye, A. Arnould, A. Ghazisaeidi, D. Le Gac and J. Renaudier, "Experimental Prediction and Design of Ultra-Wideband Raman Amplifiers using Neural Networks," *in Optical Fiber Communications Conference and Exhibition* (2020).
36. M. Ionescu, A. Ghazisaeidi, J. Renaudier, P. Pecci and O. Courtois, "Design Optimisation of Power-Efficient Submarine Line through Machine Learning," in *Conference on Lasers and Electro-Optics* (2020)
37. J. Cho, S. Olsson, E. Burrows, G. Raybon, R. Ryf, N. Fontaine, A. Chraplyvy, P. Winzer, S. Chandrasekhar, E. Sula, J-C. Antona, S. Grubb, "Supply-Power-Constrained Cable Capacity Maximization Using Multi-Layer Neural Networks," in *J. Lightwave Technol.*, vol. 38, no. 14, pp. 3652-3662 (2020).
38. M Ionescu, T Frisch, E. Sillekens and P. Bayvel, “Artificial Intelligence or Real Engineer, which is better?”, in *SubOptic* 2019.
39. A. M. Rosa Brusin, V. Curri, D. Zibar, and A. Carena, “An ultrafast method for gain and noise prediction of Raman amplifiers,” in *European Conference on Optical Communication* (2019), paper Th.1.C.3.
40. U. C. de Moura, F. Da Ros, A. M. R. Brusin, A. Carena, and D. Zibar, "Experimental demonstration of arbitrary Raman gain–profile designs using machine learning," in Optical Fiber Communication Conference (2020), paper T4B.2.
41. A. M. R. Brusin, U. C. de Moura, A. D’Amico, V. Curri, D. Zibar, and A. Carena, "Load aware Raman gain profile prediction in dynamic multi-band optical networks," in *Optical Fiber Communication Conference* (2020), paper T4B.3.
42. D. Zibar et al., “Inverse System Design Using Machine Learning: The Raman Amplifier Case,” *J. Lightwave Technol.*, vol. 38, no. 4, pp. 736-753 (2020).
43. Y. Chen, J. Du, Y. Huang, K. Xu, and Z. He, "Intelligent gain flattening of FMF Raman amplification by machine learning based inverse design," in *Optical Fiber Communication Conference* (2020, paper T4B.1.
44. J. Zhou, J. Chen, X. Li, G. Wu, Y. Wang, and W. Jiang, "Robust, Compact, and Flexible Neural Model for a Fiber Raman Amplifier," in *J. Lightwave Technol.* 24, 2362-2367 (2006).
45. D. Zibar, A. Ferrari, V. Curri, and A. Carena, "Machine learning-based Raman amplifier design," in *Optical Fiber Communication Conference* (2019), paper M1J.1.
46. J. Chen and H. Jiang, "Optimal Design of Gain Flattened Raman Fiber Amplifiers Using a Hybrid Approach Combining Randomized Neural Networks and Differential Evolution Algorithm," in *IEEE Photonics Journal*, vol. 10, no. 2, pp. 1-15 (2018).
47. Y. You, Z. Jiang and C. Janz, "Machine Learning-Based EDFA Gain Model," in *European Conference on Optical Communication* (2018), paper Mo3E.5.
48. S. Zhu, C. Gutterman, A. Diaz Montiel, J. Yu, M. Ruffini, G. Zussman, and D. Kilper, “Hybrid Machine Learning EDFA Model”, in *Optical Fiber Communication Conference* (2020), paper T4B.4.

Emmanuel Seve () received his Ph.D. degree in physics from Bourgogne University, France. Between 1999 and 2000, he was a postdoctoral fellow at Aston University in Birmingham, UK. In July 2000,

Dr. Seve joined Alcatel (then Alcatel-Lucent and now Nokia) Bell Labs as a research engineer. His primary research was focusing on physical impairments modeling and now its application on optical and intelligent networks modeling using machine-learning techniques.

Jelena Pesic () received the Ph.D. degree from the University of Bretagne Sud in collaboration with France Telecom-Orange Labs, France in 2012. From 2012 to 2014, she was a postdoctoral fellow at INRIA and Telecom Bretagne working on European project SASER. She received a best paper award at the IEEE ONDM conference in 2011. After joining Alcatel-Lucent (now Nokia) Bell Labs in 2014, she focused on dynamic elastic networks dimensioning and techno-economic studies. Her main areas of research interest include intelligent optical networks, including core and metro networks.

Yvan Pointurier () received a Ph.D. from the University of Virginia, USA in 2006. Between 2006 and 2009, he was a postdoctoral fellow at McGill University in Montreal and then a senior researcher at AIT, Greece. In 2009, Dr. Pointurier joined Alcatel-Lucent (now Nokia) Bell Labs as a research engineer and was at the head of the "Dynamic Optical Networking and Switching" department at Nokia Bell Labs until 2020. He joined Huawei Technologies as a research team leader. Dr. Pointurier has authored or co-authored more than 15 European and US patents, and over 90 technical papers in leading journals, key conferences (OFC, ECOC, ACM Internet Measurement Conference, IEEE Infocom, ICC, Globecom), and book chapters. He received a best paper award at the IEEE ICC conference in 2006 and an IEEE Communication Letters Exemplary Reviewer award in 2014 and 2016 (top 3% of the reviewers). Dr. Pointurier has been a TPC member for IEEE ICC, the flagship IEEE conference on communications, since 2007.